Geophysical Research Letters

RESEARCH LETTER
10.1029/2019GL086604

# Elastic Fault Interactions and Earthquake Rupture Along the Southern Hellenic Subduction Plate Interface Zone in Greece

**Vasso Saltogianni[1], Vasiliki Mouslopoulou[2], Onno Oncken[1], Andrew Nicol[3], Michail Gianniou[4,5], and Stelios Mertikas[6]**

[1]Helmholtz Centre Potsdam, GFZ German Research Centre for Geosciences, Potsdam, Germany, [2]Institute of Geodynamics, National Observatory of Athens, Athens, Greece, [3]School of Earth and Environment, University of Canterbury, Christchurch, New Zealand, [4]Hellenic Cadastre, Athens, Greece, [5]School of Engineering, University of West Attica, Athens, Greece, [6]School of Mineral Resources Engineering, Geodesy and Geomatics Engineering Lab, Technical University of Crete, Chania, Greece

**Abstract** The importance of splay-thrust faults in subduction seismogenesis is increasingly acknowledged; however, their elastic interaction with the plate interface remains unclear. Here, we use GPS velocities, constrained by millennial fault slip rates, to study elastic fault-interactions between the plate interface and its upper-plate splay-thrust faults from the southern Hellenic Subduction System (HSS). We find that, despite its largely aseismic character, the HSS plate interface zone is kinematically segmented, with slip rate deficits locally reaching ~85% and ~45% of the plate convergence rate on the western and eastern segments, respectively, and on structures different from those that ruptured historically. Although western Crete has been more active seismically during late Holocene, we find that the eastern HSS has higher seismic potential for large-magnitude ($M > 6$) earthquakes and its interface zone is closer to failure. Elastic fault interactions are responsible for both significant intersegment variability in strain accumulation and uniformity in earthquake rupture segmentation along the HSS over millennial timescales.

**Plain Language Summary** The southern Hellenic Subduction System (HSS) hosted at 365 CE the greatest earthquake (~$M$8.3) ever recorded in the Mediterranean. This earthquake, unlike other large subduction earthquakes, did not rupture the main contact between the two sliding tectonic-plates (i.e., the plate interface) but, instead, it was generated on a steep large fault that branches upward from the plate interface to extend within the upper plate. As the main plate interface fault and its branch(es) are linked at depth and accumulate strain interdependently, rupture on one controls the locus and timing of rupture on neighboring faults. Thus, to better assess the seismic hazard along the HSS it is crucial to chart and quantify the amount of strain stored on each of these structures. Here, we use dense GPS data and normal fault displacements to derive, for the first time, a detailed "locking" map of each fault in the southern HSS. We find that the western and eastern sections of the HSS rupture during different earthquakes (HSS is segmented), with these earthquakes breaking interchangeably the plate interface and its branches. Further, we find that although western HSS has been more active seismically in the last 5,000 years, the eastern HSS has higher potential for $M > 6$ earthquakes in the near future.

**Key Points:**
- Spatially variable elastic strain accumulation in the Hellenic plate interface zone produces persistent earthquake rupture segments
- Slip rate deficit up to 85% and 45% of the plate convergence rate on the western and eastern segments of the interface zone, respectively
- Potential for large-magnitude ($M > 6$) earthquakes in the eastern Hellenic margin elevated compared to that in the western

**Supporting Information:**
- Supporting Information S1

**Correspondence to:**
V. Saltogianni,
salto@gfz-potsdam.de

**Citation:**
Saltogianni, V., Mouslopoulou, V., Oncken, O., Nicol, A., Gianniou, M., & Mertikas, S. (2020). Elastic fault interactions and earthquake rupture along the southern Hellenic subduction plate interface zone in Greece. *Geophysical Research Letters*, *47*, e2019GL086604. https://doi.org/10.1029/2019GL086604

Received 16 DEC 2019
Accepted 18 MAY 2020
Accepted article online 9 JUN 2020
Corrected 27 JUL 2020

This article was corrected on 27 JUL 2020. See the end of the full text for details.
Correction added on 16 SEP 2020, after first online publication: Projekt DEAL funding statement has been added.



## 1. Introduction

The world's largest earthquakes occur on plate interface faults along subduction zones (McCaffrey, 2008; Moreno et al., 2010; Tichelaar & Ruff, 1993). However, in many subduction zones worldwide the up-dip end of the plate interface may branch upward into one or more large thrust faults to form a complex zone within the upper-plate (e.g., Farías et al., 2011; Melnick et al., 2012; Mouslopoulou et al., 2015, 2016, 2019; Park et al., 2002; Priest et al., 2010; Singh et al., 2011; Wilson et al., 2006) (Figure 1a). These upper-plate splay faults intersect and interact with the subduction plate interface thrust to form a single coherent fault system (Walsh & Watterson, 1991), here referred to as the "plate interface zone," which accumulates displacement as a result of plate convergence (Figure 1a).

The complex fault geometries that characterize *plate interface zones* raise the question of how the plate interface thrust and its major splay-thrust faults interact through large-magnitude earthquakes to accommodate

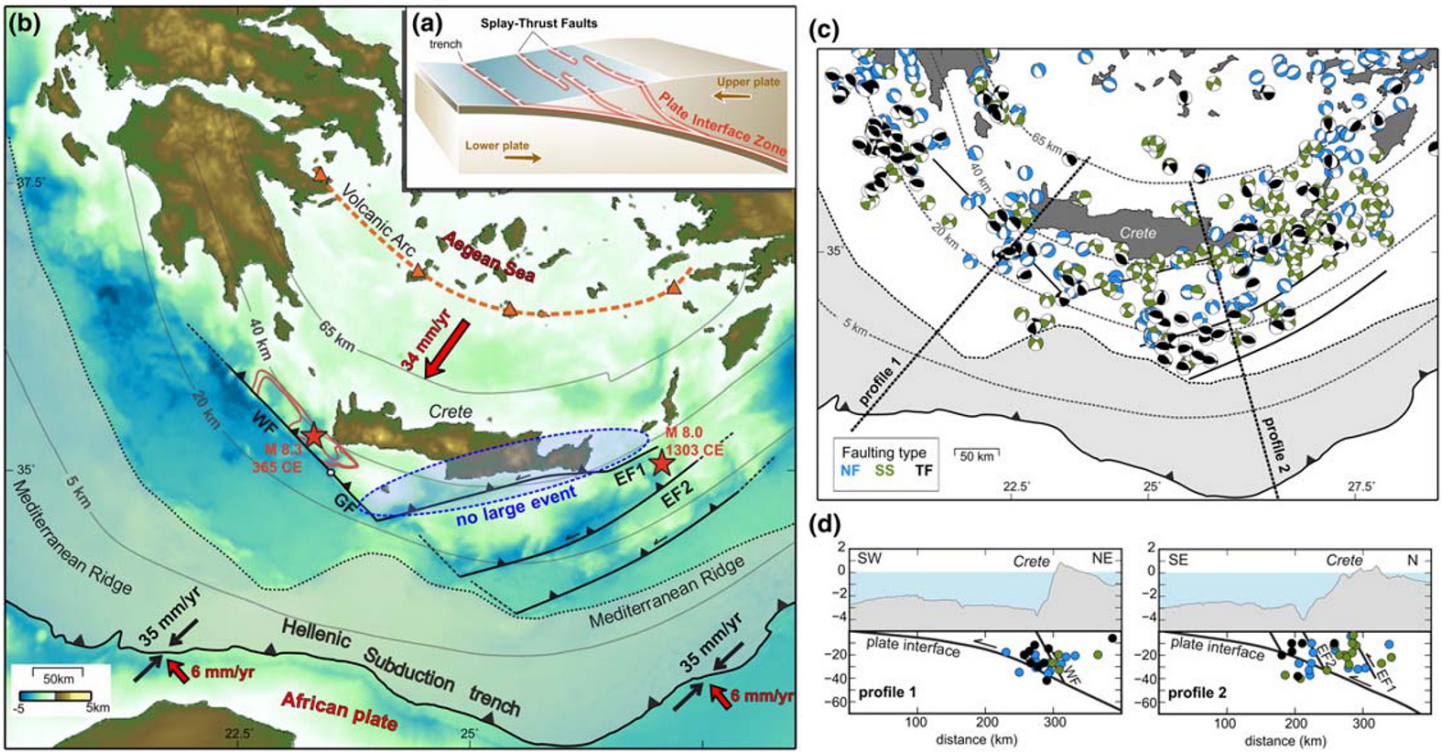


**Figure 1.** (a) The "plate interface zone" as defined by the plate interface proper and its splay-thrust faults. Each fault within this zone is a component of a kinematically coherent system, the growth of which is driven by the relative plate motion. (b) The Hellenic Subduction System (HSS) and main forearc splay-thrust faults offshore Crete. Plate interface depth contours are shown by gray lines (Bocchini et al., 2018). Red stars indicate two $M \geq 8$ events that ruptured the western and eastern segments of the HSS during the last ~2 millennia (365 CE and 1,303 CE). The 10 and 20 m coseismic slip contours produced by the 365 CE event are also shown (Mouslopoulou et al., 2015). The 4,000 year-long seismic gap observed along eastern Crete (Mouslopoulou et al., 2015) is also marked. Red arrows indicate the movement of the overriding and lower plate with respect to stable Eurasia. Black arrows indicate the convergence rate between the Africa and Eurasian plates. (c) Distribution of focal mechanisms for the period 1976–2010 along the HSS (Konstantinou et al., 2017), color coded as per fault type (see legend) and in (d) they are presented in depth sections along Profiles 1 and 2. (WF = Western fault, EF = Eastern fault, GF = Gavdos fault; adopted from Mouslopoulou et al., 2015).

plate convergence. Large tsunamigenic earthquakes can originate from steep splay faults and not from the plate interface proper (e.g., Hsu, 2006; Mouslopoulou et al., 2015; Shaw et al., 2008), while increasing evidence suggests that the timing of large subduction earthquakes can be influenced by rupture of thrust faults in the overriding plate (e.g., Barnes et al., 2002; Melnick et al., 2009; Mouslopoulou et al., 2016). The key role of these splay-thrust faults and their interaction with the subduction plate interface itself was recently highlighted by the 2016 *M*7.8 Kaikōura earthquake (New Zealand), where upper-plate faulting triggered up to 6 m of coseismic slip on the plate interface (Mouslopoulou et al., 2019). Hence, although it is increasingly acknowledged that splay fault systems have a direct impact on the kinematics and stress state of the plate interface, it is still unclear how elastic strain accumulates and/or is partitioned interseismically within such complex fault zones.

Here, we capture, for the first time, the spatial and temporal accumulation of elastic strain on multiple faults within a plate interface zone (Figure 1a). We focus on the southern Hellenic Subduction System (HSS) (Figure 1b), where the greatest earthquake (*M*8.3) and tsunami recorded in the Mediterranean was mainly produced by rupture on a splay-thrust fault (Flemming, 1978; Mouslopoulou et al., 2015; Pirazzoli et al., 1982; Shaw et al., 2008; Stiros & Drakos, 2006). This earthquake, which occurred at 365 Common Era (CE) and produced up to 10 m of coseismic uplift in western Crete, resulted from the active subduction of the African plate beneath the Eurasian plate at rates of ~35–40 mm/yr (Figure 1b; McClusky et al., 2000). Despite the detailed documentation of the coseismic slip pattern produced by this fault during the 365 CE event (Figure 1b), little is known about its current elastic strain accumulation and its potential interaction with the plate interface proper. Little is also known about the interseismic strain accumulation along the

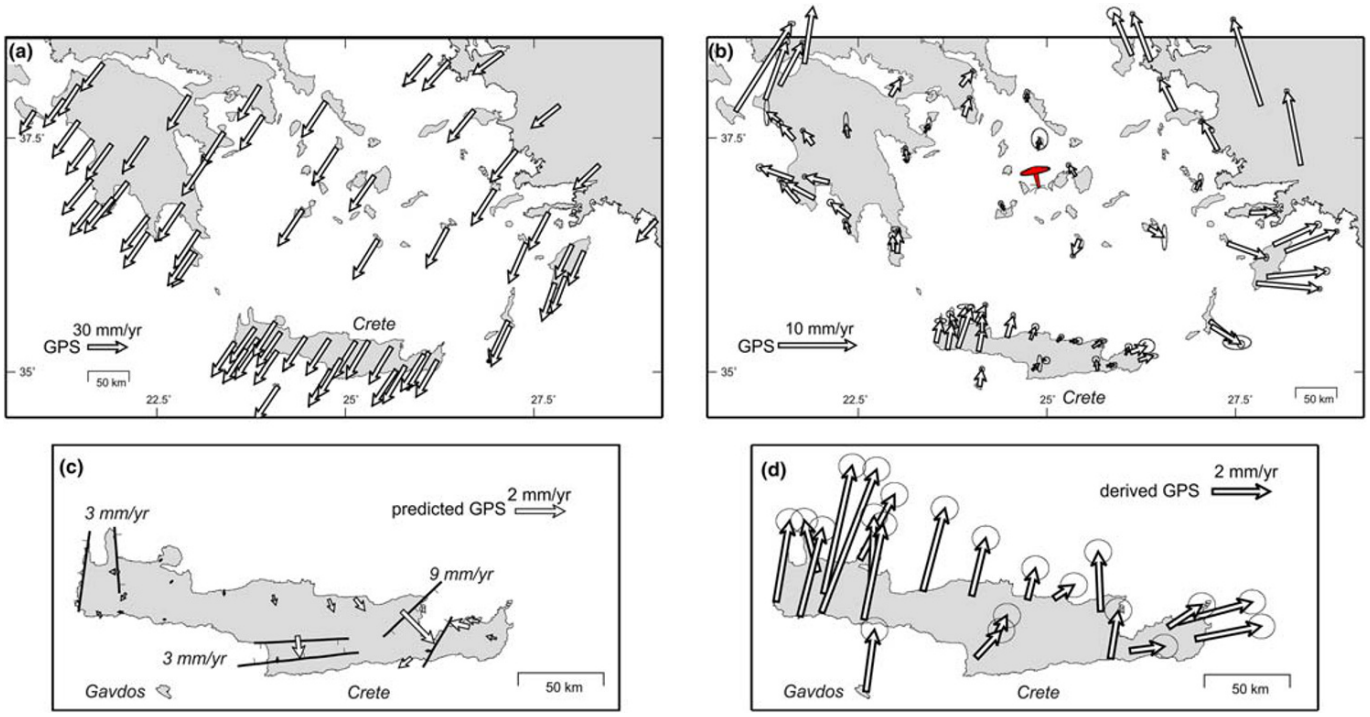


**Figure 2.** Horizontal GPS velocities with respect (a) to Eurasia and (b) to Eurasia-Aegean along the HSS. (c) Predicted horizontal velocities on the islands of Crete and Gavdos due to upper-plate normal faulting as constrained by empirical measurements (Nicol et al., 2020). Normal faults are schematic and indicate the main locus of upper-plate deformation. (d) Horizontal velocities after the component of normal-faulting has been removed from the GPS signal.

eastern segment of the HSS, where another ~*M*8 earthquake occurred in 1303 CE (Guidoboni & Comastri, 1997) (Figure 1b), most likely due to rupture on the plate interface itself (Papadopoulos, 2011).

To quantify the degree of interseismic locking on individual faults within the southern Hellenic plate interface zone and capture possible elastic fault interactions, we analyze geodetic data from a dense network of 21 permanent GPS stations located on the islands of Crete and Gavdos (Figure 2c and 2d). Interpretation of GPS data is further constrained by millennial displacement-rates from normal faults on Crete (Nicol et al., 2020). Our analysis shows spatially variable strain accumulation and reveals locations within the plate interface zone that are presently locked and accumulate significant elastic strain (i.e., have a high slip-rate deficit) that may be released in future large-magnitude earthquakes. Elastic strains are interpreted to reflect fault interactions and earthquake-rupture segmentation along the southern HSS that persists over multiple earthquake-cycles (Figures 3 and 4).

## 2. Plate Interface Zone Deformation

### 2.1. Modeling of Slip Rate Deficit

We study the Hellenic plate interface zone and model the distribution of slip rate deficit on splay faults and the subduction interface using GPS-derived displacement rates from 21 permanent stations located on the islands of Crete and Gavdos. Collectively, data span the period between 2002 and 2018 (Figure 2; Table S1 in the supporting information). To account for the Hellenic slab-rollback (Royden, 1993), the westward extrusion of the Anatolian Plate (McClusky et al., 2000; McKenzie, 1972; Reilinger et al., 2006), and the component of normal fault slip recorded by the GPS data, we sequentially "clean" the GPS signal, first by subtracting the Eurasian-fixed motion and then calculating the velocities with respect to stable northern Cyclades (see red pin in Figure 2b) and, subsequently, by subtracting the extension produced on Crete over millennial timescales due to normal faulting on Crete (Nicol et al., 2020) (Figure 2c). The impact of offshore normal faulting on the resolved velocities on Crete and Gavdos is negligible (Figure S6) and therefore not included in the final inversion. The remaining GPS signal (Figure 2d) records the requisite deep-seated

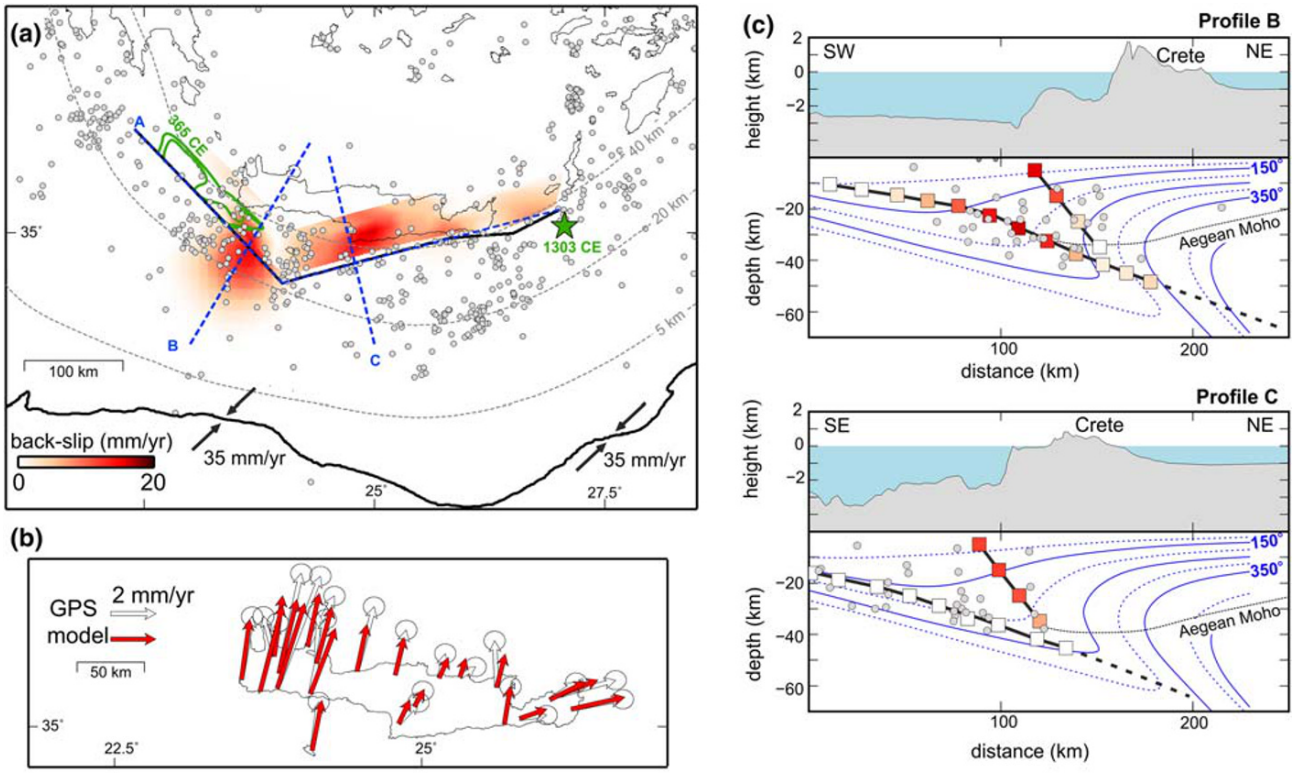


**Figure 3.** (a) Distribution of the total slip rate deficit within the plate interface zone of the southern HSS. Relocated seismicity ($M > 4$; depth < 60 km; EHB catalog) for the period 1970–2008 is corrected for depth based on Meier et al. (2004). Profile A is illustrated in Figure 4. (b) Measured (white) and modeled (red) GPS velocities. (c, d) The distribution of slip rate deficit within the plate interface zone along the profiles B and C (Figure 3a). The topography, the thermal gradient of the subducting slab (Bocchini et al., 2018) and the Aegean Moho (Sodoudi et al., 2015) are shown.

deformation, which is subsequently used to estimate the slip-rate deficit within the plate interface zone (Figure 1a).

Slip at depth is modeled using the back-slip approach of Savage (1983) and assuming an elastic homogeneous half-space (Okada, 1985). Modeled fault geometries along the southern HSS were constrained by published data including seismic tomography (Halpaap et al., 2018), relocated seismicity (Bocchini et al., 2018), focal mechanisms (Shaw & Jackson, 2010), seismic-reflection data (Kokinou et al., 2012), uplifted paleoshorelines (Mouslopoulou et al., 2015), and offshore bathymetry (https://portal.emodnet-bathymetry.eu/?menu=19). Overall, our preferred model involves slip on four principal slip surfaces: the plate interface proper and three thrust faults that splay from the plate interface at ~40 km depth (see Figure 1b; Mouslopoulou et al., 2015). For further details on the analysis and modeling of the geodetic data and all associated sensitivity tests, refer to the supporting information.

### 2.2. Distribution of Interseismic Locking

We derive our preferred 3-D fault configuration and interseismic locking by running a range of kinematic scenarios and testing different geometries for the smallest model misfits (Figure 3, and Figures S4 and S5). Our best fit model reveals two main areas of interseismic locking in the southern HSS: one offshore western Crete (and close to the southern tip of the 365 CE earthquake; Figure 3a) and another south and beneath central-eastern Crete (Figure 3a). The region between those two "locked" zones is characterized by low interseismic strain accumulation. Examination of Figure 3a shows that the peripheries of the two main asperities are bounded by microseismicity while internally the "locked" zones appear to accommodate little (or no) seismicity. The relationship between locking and seismicity is further highlighted by the negative correlation between seismic and geodetic moment accumulation along the subduction margin (Figure 4d). Such patterns are often interpreted to indicate velocity-strengthening patches which are prone to creep and associated microseismicity, with locked zones undergoing velocity-weakening (Moreno et al., 2011). Similar

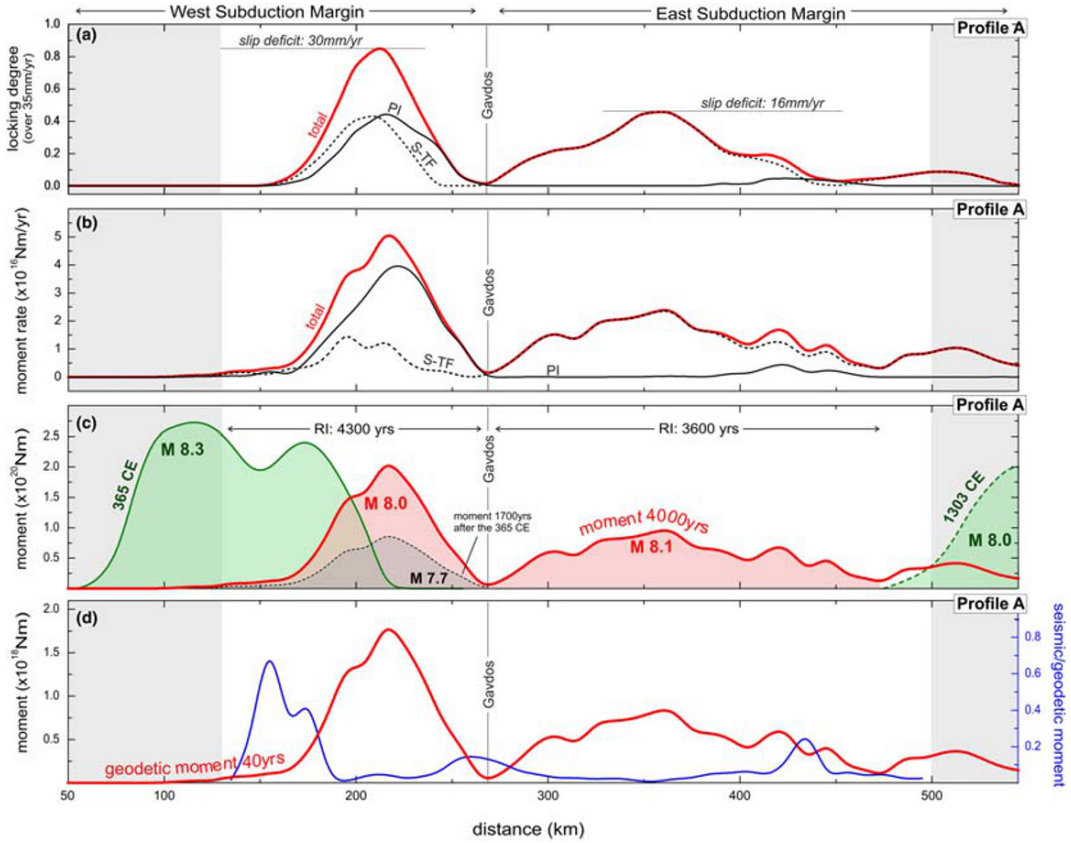


**Figure 4.** Distribution of the (a) degree of locking and (b) geodetic moment rate along Profile A (Figure 3a). The black solid and dashed lines represent strain accumulated on the plate interface (PI) and splay-thrust faults (STF), respectively, whereas the red line shows the total rate accumulated within the plate interface zone. (c) Geodetic moment accumulated within the plate interface zone during the last 4,000 years is shown by red line. This moment corresponds to a ~*M*8 earthquake for each of the two asperities. The moment deficit accumulated during the last 1,700 years in western Crete (e.g., since the 365 CE event) is illustrated by the black dashed line and corresponds to a *M*7.7 earthquake. The coseismic moment distribution of the two $M > 8$ historic earthquakes in western and eastern Crete are indicated by green shadings. (d) Red line indicates the geodetic moment accumulated over the last ~40 years of instrumentally recorded seismicity (1970–2010). The blue line indicates the ratio of seismic to geodetic moment. Gray areas at either end of Profile A denote areas where model resolution is low.

patterns have been documented along the Nazca plate in South Central Chile (Metois et al., 2012; Moreno et al., 2011) and Peru (Chlieh et al., 2011).

The average slip rate deficits are 5 and 7 mm/yr on the western and eastern regions, respectively. These deficits account for ~15% and ~20% of the total African-Eurasian convergence-rate (~35 mm/yr), which is consistent with the <20% locking values proposed in the literature (Floyd et al., 2010; Reilinger et al., 2010; Shaw & Jackson, 2010; Vernant et al., 2014) assuming, however, a uniform locking distribution. Instead, by allowing the slip accumulation to vary with depth, for the first time we derive the spatial distribution and maximum values of locking on each structure of the plate interface zone (Figure 3).

A maximum slip rate deficit (30 mm/yr) is modeled on the western locked patch at depths ranging from 5 km (splay-thrust fault) to 27 km (plate interface proper) (Figures 3c and 4a). Locking on this asperity, which may locally accommodate up to 85% of the total convergence rate (i.e., 30 of 35 mm/yr), appears to be equally distributed between the splay-thrust fault and the plate interface itself (Figures 3c and 4a). By contrast, the plate interface proper along the eastern asperity appears to be mainly uncoupled, with elastic strain (<16 mm/yr and <45% of the plate motion) being accumulated on a splay-thrust fault, immediately south of Crete and at depths ranging from ~5 to 35 km (Figures 2c and 4a). However, as the plate interface and splay-thrust faults are modeled as a single coherent fault-system that collectively accommodates convergence-related strain, we cannot exclude the possibility that some strain in the east is unresolved by the model and accumulated on

the plate interface proper (Figures S4a and S4c). Stronger maximum interseismic locking on the western asperity compared to the eastern (85% vs. 45%), is consistent with the eastward decrease in topography and increase in normal faulting (Nicol et al., 2020). The patterns of topography could reflect greater shortening in the upper plate above the zone of stronger maximum interseismic locking in the west (compared to the east) and may indicate that the GPS signal records processes that operate on timescales of millennia to millions of years (Mouslopoulou et al., 2015; Veliz et al., 2018).

The plate interface proper accommodates strain only at depths >15 km (Figure 3c), with its upper extent modeled to creep aseismically. The available GPS data cannot resolve near trench deformation, but the up-dip end of the locked zone can be inferred from the lack of seismicity along the Mediterranean Ridge (Figures 1b, S3, and S7). The down-dip end of the locked zone on both asperities occurs at 35–40 km, consistent with observations from other subduction margins globally (Moreno et al., 2011; Wallace et al., 2004).

To independently assess the depth distribution of the modeled locked zone, we superimpose the thermal gradient of the Hellenic slab in the profiles of Figure 3c (Bocchini et al., 2018) and the Moho depth of the continental Aegean upper plate (Sodoudi et al., 2015). Comparison shows that the down-dip and up-dip limits of both locked patches occur at ~350°C and ~100°C, respectively, while the Aegean Moho abuts against the inferred down-dip end of the locked interface zone (Figure 3c); these features collectively characterize subduction systems worldwide and, thus, independently validate our best fit model (Hyndman, 2007; Oleskevich et al., 1999).

### 2.3. Interseismic Fault Interactions

Understanding the kinematic interdependency of interseismic strain accumulation on the faults which are elements of a single subduction system (Figure 1a), and the impact that these interactions may have on the recurrence of large-magnitude earthquakes, is crucial for the characterization of seismic hazard. Along the southern HSS this is particularly important as the plate interface zone comprises a multielement fault system, with the kinematic interdependence of faults controlling the locus and timing of future large earthquakes in the eastern Mediterranean (Mouslopoulou et al., 2015, 2016) (Figure 1a).

The distribution of geodetic moment rate along each structure of the southern HSS is summarized in Figure 4b. Data suggest a clear segmentation in elastic strain accumulation between the western and eastern section of the HSS, with the western margin locally being twice as locked (< ~85%) compared to the eastern (< ~45%). Strong locking in the west results from elastic strain being stored on both the plate interface and its splay-thrust fault (Figures 3a, 4b, and 4c) whereas in the east, strain is accumulated primarily on the splay-thrust fault (Figure 4a and 4b). Thus, earthquake rupture segmentation is suggested for the plate interface zone which is only strongly locked along the principal slip surface (plate interface proper) in the west, with the two splay-thrust faults accommodating elastic strain interdependently (note the two triangular moment-rate profiles along the southern HSS which are indicative of the growth of individual faults; Manzocchi et al., 2006) (Figure 4b).

As heterogeneities in fault strength and stress conditions have a primary impact on the frequency, timing, and dimensions of earthquake ruptures (Scholz, 2019), it is important to evaluate, based on the current distribution of elastic strain, the seismic potential of the southern HSS. To achieve this, we use a constant geodetic moment-rate to calculate the interseismic moment accumulated within the plate interface zone since 365 CE in the west, and over the last 4,000 years in the east (Figure 4c). The accumulated moment beneath central eastern Crete (e.g., the region that has not hosted a large-subduction earthquake in the late-Holocene) is approximately equivalent to a ~$M$8.1 earthquake, while on the western asperity the accumulated moment since the 365 CE is equivalent to a ~$M$7.7 earthquake (Figure 4c). This is also reflected in the average earthquake recurrence intervals for the eastern and western HSS which are independently calculated to be ~3,600 and ~4,300 years, respectively (Figure 4c). It is also possible that the accumulated elastic strain may be released by a series of more frequent moderate-sized ($M$6–7) events, similar to those comprised the 2008 Mw6.9 Methoni earthquake sequence (Howell et al., 2017). Overall, the above calculations suggest that, although western Crete has been more active seismically in late Holocene, seismic and tsunami hazard may be more elevated in the eastern section of the HSS.

Interestingly, the maximum elastic strain within the western asperity does not coincide spatially with the rupture area of the 365 CE event but, instead, is shifted towards the southern tip of the 365 CE rupture

(Figure 4c). This southward shift can be rationalized if we consider that stress transfer often results in initiation of rupture at the tips of past ruptures (Stein, 1999). The strain along the northern tip of the 365 CE rupture cannot be adequately resolved by the current GPS data (see gray shading in Figure 4c); however, given the lack of microseismicity in this region (Figure 3a), strain accumulation is possible.

## 3. Short-Term Versus Long-Term Earthquake Kinematics

The southern HSS is currently accumulating elastic strain at spatially variable rates and depths along individual structures within the interface zone (Figures 3 and 4). A question arises as to whether these along and across system strain accumulation patterns persist over multiple earthquake cycles (e.g., >10 kyr) or are ephemeral features.

By comparing the current pattern of interseismic strain accumulation with the spatial distribution of large historic earthquakes within the interface zone, we observe significant variability in the loci of seismic moment accumulation/release through time. For example, the last subduction earthquake on the western HSS (e.g., the 365 CE event) occurred on a splay-thrust fault, with little contribution of the plate interface (Mouslopoulou et al., 2015; Shaw et al., 2008; Stiros, 2010). Interestingly, this thrust fault currently accumulates little strain with the majority of it being on the plate interface proper and on a neighboring thrust-fault (e.g., the Gavdos Fault; see Figures 1b and 3c). By contrast, historic information (Guidoboni & Comastri, 1997; Papadopoulos, 2011; Papazachos & Papazachou, 1997), coupled with tsunami modeling (e.g., Yolsal et al., 2007) and absence of late-Holocene uplift on eastern Crete and Kasos (Mouslopoulou et al., 2015), suggest that in the east, the *M*8 1,303 CE event was not generated by slip on the splay-thrust fault immediately south of Crete, with the plate interface being a likely candidate for this event (Figures 1b and 4c). Whether another splay-thrust fault, outside the GPS data resolved area (see, e.g., fault EF2 in Figure 1), is responsible for the 1,303 CE event (e.g., England et al., 2015) remains unclear. Nevertheless, if that was the case, some subsidence on Crete and/or Kasos would be expected. Interestingly, the section of the plate interface in the area of the 1,303 CE event appears currently to creep, with elastic strain primarily stored on the overlying thrust-fault (Figure 3c. 4b, and 4c). Even if strain is accommodated on different structures of the interface zone during consecutive earthquake-cycles, the region south of Gavdos Island appears to be a major boundary to earthquake-rupture propagation that also coincides spatially with a significant change in the margin's strike from NW-SE to NE-SW (Figure 1b).

Along-margin variability in the interseismic strain accumulation is also supported by the distribution of late-Pleistocene paleoshorelines on Crete which, together with numerical models, suggest: (a) different subduction-earthquake history for western and eastern Crete during the late-Holocene (0–5 kyr); (b) uniformity in the uplift accrued along Crete during the last ~50 kyr, and (c) uplift was primarily achieved by earthquakes that ruptured individual splay-thrust faults south of Crete, with limited contribution from plate interface slip (e.g., Mouslopoulou et al., 2015). These findings are consistent with the strain-accumulation patterns arising independently from the modeling of geodetic data (Figures 3 and 4). Long-term earthquake rupture segmentation is further supported by the ~4 kyr average recurrence interval for *M*8 earthquakes calculated for the southern HSS using geodetic data (see section 2.3 and Figure 4c) which is broadly consistent with the ~5 kyr recurrence of *M*8 earthquakes calculated from late-Pleistocene paleoshorelines (Mouslopoulou et al., 2015; Shaw et al., 2008).

The kinematic segmentation observed along the southern HSS over short (geodetic) and long (geological) timescales, is also reflected in the pattern of instrumental seismicity (Konstantinou et al., 2017; Shaw & Jackson, 2010; Taymaz et al., 1990). Indeed, in the southeast HSS a greater number of shallow normal and strike slip events is recorded compared to the southwest, where focal mechanisms reveal predominance of deep thrust faulting (Figures 1d and S7) (Konstantinou et al., 2017; Meier et al., 2004). These mechanisms are consistent with the orientation of the plate convergence vectors, which are margin-normal south of western Crete and oblique (40–50$^{o}$) south of eastern Crete (Figures 1b and 2d).

Thus, kinematic data from various datasets, that collectively span timescales that range from seconds to thousands of years, suggest that large-magnitude earthquakes rupture either side of the southern HSS during distinct events. They also suggest that this along-margin kinematic segmentation is likely produced by earthquakes that rupture one or more faults across the plate interface zone. Hence, elastic fault interactions between synchronous operating elements of a plate interface zone produce variable strain accumulation

(and associated rupture arrest) within each segment and uniform millennial displacement patterns along the entire southern HSS.

## 4. Seismic-Slip Versus Aseismic Creep

Despite the occurrence of large ($M > 7$) subduction earthquakes along the HSS, the majority of the plate motion is accommodated aseismically (Floyd et al., 2010; Reilinger et al., 2010; Shaw & Jackson, 2010; Vernant et al., 2014; this study). By summing the amount of strain stored elastically within the plate interface zone (this study) with that converted onto permanent deformation in the upper-plate (Nicol et al., 2020), we can estimate the percentage of plate convergence that is accommodated seismically and/or aseismically along the various sections of the southern HSS. We find (see section 2.2) that, on average, ~5 and ~7 mm/yr are stored elastically within the western and eastern plate interface zones, respectively. At the same time, normal faulting onshore Crete accommodates summed displacement rates of ~3 and ~12 mm/yr in western and eastern Crete, respectively (Nicol et al., 2020). This collectively suggests that ~78% ($5 + 3 = 8$ mm/yr of 35 mm/yr) of the African-Eurasian plate convergence in the west and ~46% ($7 + 12 = 19$ mm/yr of 35 mm/yr) in the east is aseismic or that the seismic potential in the east exceeds by about a factor of two that in the west (54% vs. 22%). The latter mainly reflects the significance of normal faulting in the east of Crete compared to the west (12 vs. 3 mm/yr; Nicol et al., 2020) and less so the contribution of large-subduction earthquakes. On the other hand, aseismic deformation along the southern HSS is assumed to be accommodated by creep within the interface zone; however, episodes of slow-slip events cannot be excluded (e.g., Araki et al., 2017; Dragert et al., 2001; McCaffrey, 2008; Wallace & Beavan, 2010). High creeping to locking ratios have been attributed to subductions characterized by rough seafloor relief (Lallemand et al., 2018; van Rijsingen et al., 2019; Wang & Bilek, 2014), variations in fictional properties (Moreno et al., 2014; Perfettini et al., 2010) and/or variations of topography/bathymetry (Song & Simons, 2003). Which of the above (if any) mechanisms operate along the southern HSS remains currently unconstrained.

Overall, our analysis signifies the short-term variability in the locking pattern along the southern HSS, with strain being interdependently accommodated on individual structures of the interface zone, and persistent long-term earthquake rupture segmentation between the western and eastern margin. It also highlights that the eastern segment of the HSS has both higher seismic potential for large-magnitude ($M > 6$) earthquakes and that its interface zone is closer to failure.

**Acknowledgments**

V. S. was supported by an Alexander Von Humboldt Postdoctoral Fellowship, while V. M. acknowledges support from an internal NOA Fellowship. We thank Xenophon Frantzis (TUC) for processing the raw GPS data from the permanent stations operated by the Technical University of Crete. We also acknowledge GPS station raw data providers to Nevada Geodetic Laboratory (NGL): National Observatory of Athens (NOA), National Technical University of Athens (NTUA), University of Patras (UPatras) and Metrica S.A. from Greece; General Directorate of Mapping (GDM) from Turkey; Massachusetts Institute of Technology (MIT), Georgia Institute of Technology (Georgia Tech) and UNAVCO from the USA; University of Oxford and COMET from the UK. We are grateful to the Editor Gavin Hayes and two anonymous reviewers for their constructive comments. We also thank Marcos Moreno, Jonathan Bedford, Sofia Kufner (GFZ, Potsdam), and Gian-Maria Bocchini (Bochum University) for helpful discussions. Open access funding enabled and organized by Projekt DEAL.

## Data Availability Statement

Available data from this work are archived in https://zenodo.org/record/3564673#.Xe4NG-hKibh (doi:10.5281/zenodo.3564673).

## References

Araki, E., Saffer, D. M., Kopf, A. J., Wallace, L. M., Kimura, T., Machida, Y., et al. (2017). Recurring and triggered slow-slip events near the trench at the Nankai trough subduction megathrust. *Science*, *356*(6343), 1157–1160. https://doi.org/10.1126/science.aan3120

Barnes, P. M., Nicol, A., & Harrison, T. (2002). Late Cenozoic evolution and earthquake potential of an active listric thrust complex above the Hikurangi subduction zone, New Zealand. *GSA Bulletin*, *114*(11), 1379–1405. https://doi.org/10.1130/0016-7606(2002)114%3C1379:LCEAEP%3E2.0.CO;2

Bocchini, G. M., Brustle, A., Becker, D., Meier, T., van Keken, P. E., Ruscic, M., et al. (2018). Tearing, segmentation, and back stepping of subduction in the Aegean: New insights from seismicity. *Tectonophysics*, *734-735*, 96–118. https://doi.org/10.1016/j.tecto.2018.04.002

Chlieh, M., Perfettini, H., Tavera, H., Avouac, J. P., Remy, D., & Nocquet, J. M. (2011). Interseismic coupling and seismic potential along the Central Andes subduction zone. *Journal of Geophysical Research*, *116*, B12405. https://doi.org/10.1029/2010JB008166

Dragert, H., Wang, K., & James, T. S. (2001). A silent slip event on the deeper Cascadia subduction interface. *Science*, *292*(5521), 1525–1528. https://doi.org/10.1126/science.1060152

England, P., Howell, A., Jackson, J., & Synolakis, C. (2015). Palaeotsunamis and tsunami hazards in the eastern Mediterranean. *Philosophical Transactions of the Royal Society A*, *373*(2053), 20140374. https://doi.org/10.1098/rsta.2014.0374

Farías, M., Comte, D., Roecker, S., Carrizo, D., & Pardo, M. (2011). Crustal extensional faulting triggered by the 2010 Chilean earthquake: The Pichilemu seismic sequence. *Tectonics*, *30*, TC6010. https://doi.org/10.1029/2011TC002888

Flemming, N. (1978). Holocene eustatic changes and coastal tectonics in the Northeast Mediterranean: Implications for models of crustal consumption, philosophical transactions of the Royal Society of London. *Series A, Mathematical and Physical Sciences.*, *289*(1362), 405–458. https://doi.org/10.1098/rsta.1978.0065

Floyd, M. A., Billiris, H., Paradissis, D., Veis, G., Avallone, A., Briole, P., et al. (2010). A new velocity field for Greece: Implications for the kinematics and dynamics of the Aegean. *Journal of Geophysical Research*, *115*, B10403. https://doi.org/10.1029/2009JB007040

Guidoboni, E., & Comastri, A. (1997). The large earthquake of 8 august 1303 in Crete: Seismic scenario and tsunami in the Mediterranean area. *Journal of Seismology*, *1*(1), 55–72. https://doi.org/10.1023/A:1009737632542

Halpaap, F., Rondenay, S., & Ottemöller, L. (2018). Seismicity, deformation and metamorphism in the western Hellenic subduction zone - new constraints from tomography. *Journal of Geophysical Research: Solid Earth*, *123*, 3000–3026. https://doi.org/10.1002/2017JB015154

Howell, A., Palamartchouk, K., Papanikolaou, X., Paradissis, D., Raptakis, C., Copley, A., et al. (2017). The 2008 Methoni earthquake sequence: The relationship between the earthquake cycle on the subduction interface and coastal uplift in SW Greece. *Geophysical Journal International*, *208*(3), 1592–1610. https://doi.org/10.1093/gji/ggw462

Hsu, Y.-J. (2006). Frictional afterslip following the 2005 Nias-Simeulue earthquake, Sumatra. *Science*, *312*(5782), 1921–1926. https://doi.org/10.1126/science.1126960

Hyndman, R. D. (2007). The seismogenic zone of subduction thrust faults: What we know and don't know. In *the seismogenic zone of subduction thrust faults* (pp. 15–40). Columbia University Press: New York. https://doi.org/10.7312/dixo13866-002

Kokinou, E., Tiago, A., & Evangelos, K. (2012). Structural decoupling in a convergent forearc setting (southern Crete, eastern Mediterranean). *Bulletin of the Geological Society of America*, *124*(7–8), 1352–1364. https://doi.org/10.1130/B30492.1

Konstantinou, K. I., Mouslopoulou, V., Liang, W.-T., Heidbach, O., Oncken, O., & Suppe, J. (2017). Present-day crustal stress field in Greece inferred from regional-scale damped inversion of earthquake focal mechanisms. *Journal of Geophysical Research: Solid Earth*, *122*, 506–523. https://doi.org/10.1002/2016JB013272

Lallemand, S., Peyret, M., van Rijsingen, E., Arcay, D., & Heuret, A. (2018). Roughness characteristics of oceanic seafloor prior to sub-duction in relation to the seismogenic potential of subduction zones. *Geochemistry, Geophysics, Geosystems*, *19*, 2121–2146. https://doi.org/10.1029/2018GC007434

Manzocchi, T., Walsh, J. J., & Nicol, A. (2006). Displacement accumulation from earthquakes on isolated normal faults. *Journal of Structural Geology*, *28*(9), 1685–1693. https://doi.org/10.1016/j.jsg.2006.06.006

McCaffrey, R. (2008). Global frequency of magnitude 9 earthquakes. *Geology*, *36*(3), 263–266. https://doi.org/10.1130/G24402A.1

McClusky, S., Balassanian, S., Barka, A., Demir, C., Ergintav, S., Georgiev, I., et al. (2000). Global positioning system constraints on plate kinematics and dynamics in the eastern Mediterranean and Caucasus. *Journal of Geophysical Research*, *105*(B3), 5695–5719. https://doi.org/10.1029/1999JB900351

McKenzie, D. (1972). Active tectonics of the Mediterranean region. *Geophysical Journal International*, *30*(2), 109–185. https://doi.org/10.1111/j.1365-246X.1972.tb02351.x

Meier, T., Rische, M., Endrun, B., Vafidis, A., & Harjes, H.-P. (2004). Seismicity of the Hellenic subduction zone in the area of the western and central Crete observed by temporary local seismic networks. *Tectonophysics*, *383*(3-4), 149–169. https://doi.org/10.1016/j.tecto.2004.02.004

Melnick, D., Bookhagen, B., Strecker, M. R., & Echtler, H. P. (2009). Segmentation of megathrust rupture zones from fore-arc deformation patterns over hundreds to millions of years, Arauco peninsula, Chile. *Journal of Geophysical Research*, *114*, B01407. https://doi.org/10.1029/2008JB005788

Melnick, D., Moreno, M., Motagh, M., Cisternas, M., & Wesson, R. L. (2012). Splay fault slip during the $M_w$8.8 2010 Maule Chile earthquake. *Geology*, *40*(3), 251–254. https://doi.org/10.1130/G32712.1

Metois, M., Socquet, A., & Vigny, C. (2012). Interseismic coupling, segmentation and mechanical behavior of the Central Chile subduction zone. *Journal of Geophysical Research*, *117*, B03406. https://doi.org/10.1029/2011JB008736

Moreno, M., Haberland, C., Oncken, O., Rietbrock, A., Angiboust, S., & Heidbach, O. (2014). Locking of the Chile subduction zone con-trolled by fluid pressure before the 2010 earthquake. *Nature Geoscience*, *7*(4), 292–296. https://doi.org/10.1038/ngeo2102

Moreno, M., Melnick, D., Rosenau, M., Bolte, J., Klotz, J., Echtler, H., et al. (2011). Heterogeneous plate locking in the South-Central Chile subduction zone: Building up the next great earthquake. *Earth and Planetary Science Letters*, *305*(3–4), 413–424. https://doi.org/10.1016/j.epsl.2011.03.025

Moreno, M., Rosenau, M., & Oncken, O. (2010). 2010 Maule earthquake slip correlates with pre-seismic locking of Andean subduction zone. *Nature*, *467*(7312), 198–202. https://doi.org/10.1038/nature09349

Mouslopoulou, V., Nicol, A., Begg, J., Oncken, O., & Moreno, M. (2015). Clusters of megaearthquakes on upper plate faults control the eastern Mediterranean hazard. *Geophysical Research Letters*, *42*, 10,282–10,289. https://doi.org/10.1002/2015GL066371

Mouslopoulou, V., Oncken, O., Hainzl, S., & Nicol, A. (2016). Uplift rate transients at subduction margins due to earthquake clustering. *Tectonics*, *35*, 2370–2384. https://doi.org/10.1002/2016TC004248

Mouslopoulou, V., Saltogianni, V., Nicol, A., Oncken, O., Begg, J., Babeyko, A., et al. (2019). Breaking a subduction-termination from top to bottom: The large 2016 Kaikōura earthquake, New Zealand. *Earth and Planetary Science Letters*, *506*, 221–230. https://doi.org/10.1016/j.epsl.2018.10.020

Nicol, A., Mouslopoulou, V., Begg, J., & Oncken, O. (2020). Displacement accumulation during paleoearthquakes for active normal faults on the eastern Mediterranean island of Crete. https://doi.org/10.31223/osf.io/zqb4r

Okada, Y. (1985). Surface deformation due shear and tensile faults in a half-space. *Bulletin of the Seismological Society of America*, *75*, 1135–1154.

Oleskevich, D. A., Hyndman, R. D., & Wang, K. (1999). The updip and downdip limits to great subduction earthquakes: Thermal and structural models of Cascadia, South Alaska, SW Japan, and Chile. *Journal of Geophysical Research*, *104*(B7), 14,965–14,991. https://doi.org/10.1029/1999JB900060

Papadopoulos, G. (2011). *A seismic history of Crete, 416 pp*. Athens, Greece: Oselotos.

Papazachos, B. C., & Papazachou, C. B. (1997). *The earthquakes of Greece*. Thessaloniki: Ziti Publications. 304

Park, J. O., Tsuru, T., Kodaira, S., Cummins, P. R., & Kaneda, Y. (2002). Splay fault branching along the Nankai subduction zone. *Science*, *297*(5584), 1157–1160. https://doi.org/10.1126/science.1074111

Perfettini, H., Avouac, J.-P., Tavera, H., Kositsky, A., Nocquet, J.-M., Bondoux, F., et al. (2010). Seismic and aseismic slip on the central Peru megathrust. *Nature*, *465*(7294), 78–81. https://doi.org/10.1038/nature09062

Pirazzoli, P. A., Thommeret, J., Thommeret, Y., Laborel, J., & Montag-Gioni, L. F. (1982). Crustal block movements from holocene shorelines: Crete and Antikythira (Greece). *Tectonophysics*, *86*(1–3), 27–43. https://doi.org/10.1016/0040-1951(82)90060-9

Priest, G. R., Goldfinger, C., Wang, K., Witter, R. C., Zhang, Y., & Baptista, A. M. (2010). Confidence levels for tsunami-inundation limits in northern Oregon inferred from a 10,000-year history of great earthquakes at the Cascadia subduction zone. *Natural Hazards*, *54*(1), 27–73. https://doi.org/10.1007/s11069-009-9453-5

Reilinger, R., McClusky, S., Paradissis, D., Ergintav, S., & Vernant, P. (2010). Geodetic constraints on the tectonic evolution of the Aegean region and strain accumulation along the Hellenic subduction zone. *Tectonophysics*, *488*(1–4), 22–30. https://doi.org/10.1016/j.tecto.2009.05.027

Reilinger, R., McClusky, S., Vernant, P., Lawrence, S., Ergintav, S., Cakmak, R., et al. (2006). GPS constraints on continental deformation in the Africa-Arabia-Eurasia continental collision zone and implications for the dynamics of plate interactions. *Journal of Geophysical Research*, *111*, B05411. https://doi.org/10.1029/2005JB004051

Royden, L. H. (1993). The tectonic expression slab pull at continental convergent boundaries. *Tectonics*, *2*(2), 303–325. https://doi.org/10.1029/92TC02248

Savage, J. (1983). A dislocation model of strain accumulation and release at a subduction zone. *Journal of Geophysical Research*, *88*(B6), 4984–4996. https://doi.org/10.1029/JB088iB06p04984

Scholz, C. H. (2019). *The mechanics of earthquakes and faulting*, Cambridge, UK: Cambridge University Press. https://doi.org/10.1017/9781316681473

Shaw, B., Ambraseys, N. N., England, P. C., Floyd, M. A., Gorman, G. J., Higham, T. F. G., et al. (2008). Eastern Mediterranean tectonics and tsunami hazard inferred from the AD 365 earthquake. *Nature Geoscience*, *1*(4), 268–276. https://doi.org/10.1038/ngeo151

Shaw, B., & Jackson, J. (2010). Earthquake mechanisms and active tectonics of the Hellenic subduction zone. *Geophysical Journal International*, *181*(2), 966–984. https://doi.org/10.1111/j.1365-246X.2010.04551.x

Singh, S. C., Hananto, N. D., & Chauhan, A. P. S. (2011). Enhanced reflectivity of backthrusts in the recent great Sumatran earthquake rupture zones. *Geophysical Research Letters*, *38*, L04302. https://doi.org/10.1029/2010GL046227

Sodoudi, F., Brüstle, A., Meier, T., Kind, R., & Friederich, W. (2015). Receiver function images of the Hellenic subduction zone and comparison to microseismicity. *Solid Earth*, *6*(1), 135–151. https://doi.org/10.5194/se-6-135-2015

Song, T.-R. A., & Simons, M. (2003). Large trench-parallel gravity variations predict seismogenic behavior in subduction zones. *Science*, *301*(5633), 630–633. https://doi.org/10.1126/science.1085557

Stein, R. S. (1999). The role of stress transfer in earthquake occurrence. *Nature*, *402*(6762), 605–609. https://doi.org/10.1038/45144

Stiros, S., & Drakos, A. (2006). A fault-model for the tsunami-associated, magnitude ≥8.5 eastern Mediterranean, AD365 earthquake. *Zeitschrift für Geomorphologie Supplementband*, *146*, 125–137.

Stiros, S. C. (2010). The 8.5+ magnitude, AD365 earthquake in Crete: Coastal uplift, topography changes, archaeological and historical signature. *Quaternary International*, *216*(1–2), 54–63. https://doi.org/10.1016/j.quaint.2009.05.005

Taymaz, T., Jackson, J., & Westaway, R. (1990). Earthquake mechanisms in the Hellenic trench near Crete. *Geophysical Journal International*, *102*(3), 695–731. https://doi.org/10.1111/j.1365-246X.1990.tb04590.x

Tichelaar, B. W., & Ruff, L. J. (1993). Depth of seismic coupling along subduction zones. *Journal of Geophysical Research*, *98*(B2), 2017–2037. https://doi.org/10.1029/92JB02045

van Rijsingen, E., Funiciello, F., Corbi, F., & Lallemand, S. (2019). Rough subducting seafloor reduces interseismic coupling and mega-earthquake occurrence: Insight from analogue models. *Geophysical Research Letters*, *46*, 3124–3132. https://doi.org/10.1029/2018GL081272

Veliz, V., Mouslopoulou, V., Nicol, A., Fassoulas, B., Begg, J., & Onkcen, O. (2018). Millenial to million year normal-fault interactions on the forearc of a subduction margin, Crete, Greece. *Journal of Structural Geology*, *113*, 225–241. https://doi.org/10.1016/j.jsg.2018.05.019

Vernant, P., Reilinger, R., & McClusky, S. (2014). Geodetic evidence for low coupling on the Hellenic subduction plate interface. *Earth and Planetary Science Letters*, *385*, 122–129. https://doi.org/10.1016/j.epsl.2013.10.018

Wallace, L. M., Beavan, J., McCaffrey, R., & Darby, D. (2004). Subduction zone coupling and tectonic block rotations in the North Island, New Zealand. *Journal of Geophysical Research*, *109*, B12406. https://doi.org/10.1029/2004JB003241

Walsh, J. J., & Watterson, J. (1991). Geometric and kinematic coherence and scale effects in normal fault systems. In: Roberts, A. M., Yielding, G., Freeman, B. (Eds.), The geometry of normal faults. *Geological Society of London, Special Publication*, *56*(1), 193–203. https://doi.org/10.1144/GSL.SP.1991.056.01.13

Wallace, L. M., & Beavan, J. (2010). Diverse slow slip behavior at the Hikurangi subduction margin, New Zealand. *Journal of Geophysical Research*, *115*, B12402. https://doi.org/10.1029/2010JB007717

Wang, K., & Bilek, S. L. (2014). Invited review paper: Fault creep caused by subduction of rough seafloor relief. *Tectonophysics*, *610*, 1–24. https://doi.org/10.1016/j.tecto.2013.11.024

Wilson, K. J., Berryman, K. R., Litchfield, N. J., & Little, T. (2006). A revision of mid-late Holocene marine terrace distribution and chronology at the Pakarae River mouth, North Island, New Zealand. *New Zealand Journal of Geology and Geophysics*, *49*(4), 477–489. https://doi.org/10.1080/00288306.2006.9515182

Yolsal, S., Taymaz, T., & Yalciner, A. C. (2007). Understanding tsunamis, potential source regions and tsunami-prone mechanisms in the eastern Mediterranean. *Geological Society Special Publication*, *291*(1), 201–230. https://doi.org/10.1144/SP291.10

## Erratum

In the originally published version of this article, the authors did not acknowledge the providers of the GPS raw data, processed by the NGL and used in the study. The acknowledgements have since been corrected, and the present version may be considered the authoritative version of record.